









## RESEARCH ARTICLE

# Melt-functionalization of cellulose nanocrystals using dynamic hindered ureas

Zehra Oluz<sup>1</sup>  | Nicholas Macke<sup>1</sup>  | Sarah Candelaria<sup>2</sup>  |  
Abrianna Ambus<sup>1</sup>  | Aurora Zemborain<sup>1</sup>  | Chinwe S. Udemgba<sup>1</sup> |  
Adam M. Weiss<sup>2</sup>  | Céline Calvino<sup>1</sup>  | Stuart J. Rowan<sup>1,2,3</sup> 

<sup>1</sup>Pritzker School of Molecular Engineering, University of Chicago, Chicago, Illinois, USA

<sup>2</sup>Department of Chemistry, University of Chicago, Chicago, Illinois, USA

<sup>3</sup>Chemical and Engineering Sciences, Argonne National Laboratory, Lemont, Illinois, USA

## Correspondence

Céline Calvino and Stuart J. Rowan, Pritzker School of Molecular Engineering, University of Chicago 5640 S. Ellis Ave., Chicago, IL 60637, USA.

Email: [celine.calvino@livmats.uni-freiburg.de](mailto:celine.calvino@livmats.uni-freiburg.de); [stuartrowan@uchicago.edu](mailto:stuartrowan@uchicago.edu)

## Funding information

Division of Chemistry, Grant/Award Number: CHE-1901635; Division of Materials Research, Grant/Award Number: DMR-2011854; Swiss National Science Foundation, Grant/Award Number: P2FRP2\_181437

## Abstract

Cellulose nanocrystal (CNC)-reinforced composites are gaining commercial attention on account of their high strength and sustainable sourcing. Grafting polymers to the CNCs in these composites has the potential to improve their properties, but current solution-based synthesis methods limit their production at scale. Utilizing dynamic hindered urea chemistry, a new method for the melt-functionalization of cellulose nanocrystals has been developed. This method does not require toxic solvents during the grafting step and can achieve grafting densities competitive with state-of-the-art solution-based grafting methods. Using cotton-sourced, TEMPO-oxidized CNCs, multiple molecular weights of poly(ethylene glycol) (PEG) as well as dodecane, polycaprolactone, and poly(butyl acrylate) were grafted to the CNC surface. With PEG-grafted nanoparticles, grafting densities of 0.47 chains nm<sup>-2</sup> and 0.10 chains nm<sup>-2</sup> were achieved with 2000 and 10,000 g mol<sup>-1</sup> polymer chains respectively, both of which represent significant improvements over previous reports for solution-based PEG grafting onto CNCs.

## KEYWORDS

cellulose nanocrystals, dynamic covalent chemistry, hindered ureas, melt functionalization, polymer grafting

## 1 | INTRODUCTION

Cellulose nanocrystals (CNCs) have become an attractive, sustainable additive to provide mechanical reinforcement in polymeric materials. These bio-derived nanorods, which have dimensions of roughly 10 nm in width and 100–500 nm in length, are directly extracted from cellulosic biomass and have shown outstanding reinforcement

capabilities when used as fillers in composites.<sup>1</sup> A key challenge in accessing such nanocomposites is the ability to achieve a uniform dispersion of CNCs within a given matrix and this has limited the use of CNCs to a relatively narrow range of applications.<sup>2</sup> The poor dispersion of CNCs in many solvents or solid polymer matrices arises from the numerous hydroxyl functional groups present on the surface of the particles that make them very hydrophilic and capable of forming inter-particle hydrogen bonds. Since many potential host polymers are

Zehra Oluz and Nicholas Macke contributed equally to this study.

This is an open access article under the terms of the [Creative Commons Attribution-NonCommercial](https://creativecommons.org/licenses/by-nc/4.0/) License, which permits use, distribution and reproduction in any medium, provided the original work is properly cited and is not used for commercial purposes.

© 2024 The Author(s). *Journal of Polymer Science* published by Wiley Periodicals LLC.

hydrophobic, the inter-particle interactions between CNCs cause the formation of agglomerates, significantly impeding their ability to reinforce the host matrix.<sup>3</sup>

Surface modification of CNCs has been widely explored to overcome these dispersion issues and promote more homogenous mechanical reinforcement of the material.<sup>4</sup> Some surface modification routes utilize these interactions to physisorb or electrostatically adsorb surfactants or polymers onto CNCs.<sup>5–8</sup> Additionally, surface modification can be achieved through covalent attachment of small molecules via different chemical reactions such as esterification, etherification, silylation, amidation, and urethanization.<sup>9–11</sup> A third, widely-employed method of CNC surface modification involves the covalent grafting of polymer chains.<sup>12,13</sup> In addition to improving dispersion, such polymer-grafted nanoparticles can also show enhanced interfacial adhesion between the filler and the polymer matrix through entanglements or other matrix-filler interactions.<sup>13</sup> Depending on the grafted polymer conformation, which is a function of the polymer molecular weight and grafting density, these interactions can greatly aid both the processing and properties of the resulting nanocomposite materials.<sup>14,15</sup>

Different pathways have been developed to graft polymers on the surface of CNCs, including “grafting-to,” “grafting-from,” and “grafting-through” approaches, among others.<sup>16–18</sup> The “grafting-from” approach relies on covalent attachment of an initiator on the CNC surface and allows for initiation of the polymerization directly from the nanoparticle surface.<sup>17</sup> The advantages of “grafting-from” include synthetic simplicity and the ability to achieve relatively high surface grafting densities of 0.1 to 0.4 chains nm<sup>-2</sup>, even for high molecular weight polymers (greater than 10,000 g mol<sup>-1</sup>).<sup>19</sup> The main drawbacks of “grafting-from” methods are the challenges to characterizing the molecular weight, composition, and surface density of the grafted polymers. Additionally, these are solution-based reactions, which can limit scalability.

Comparatively, “grafting-to” methods typically involve the direct attachment of end-functionalized polymer chains to the surface of the nanocrystals.<sup>20</sup> The benefit of these methods is the ability to attach well-characterized polymer chains to CNCs, allowing for more thorough characterization of grafting density, polymer molecular weight, and brush structure. Surface brush conformation is known to play a significant role in resulting material properties, such as improved ionic conductivity<sup>21</sup> and water transport<sup>22</sup> at higher grafting densities and improved reinforcement potential with semi-dilute brush conformations.<sup>15,23</sup> Unfortunately, “grafting-to” functionalization relies on sequential attachment of polymer chains on the CNC surface. As the surface is populated, unreacted chains in solution can be sterically hindered from reacting with the surface, which can limit grafting density.

Additionally, the most common “grafting-to” methods, which include carbodiimide coupling,<sup>24</sup> epoxy ring opening,<sup>25</sup> and isocyanate-mediated grafting,<sup>26</sup> are all typically performed in solution (most commonly in water and DMF), once again limiting the use of these methods to lab-scale.<sup>13,27</sup> This use of potentially toxic solvents during the grafting reaction for both “grafting-to” and “grafting-from” techniques is antithetical to the core purpose of using sustainable nanoparticles. Thus, it is paramount to find more industrially relevant routes toward functionalization of CNCs that can achieve high grafting density with a range of polymers and molecular weights while preserving the renewable character of the nanoparticles.

One promising “grafting-to” method that has industrial relevance is the use of isocyanate moieties that can react with the hydroxyl groups on CNCs to form urethane linkages. This reaction is ubiquitous in the polyurethane industry<sup>28</sup> and has also been used to functionalize CNCs.<sup>9</sup> One limitation of this method when used with CNCs is the hygroscopic nature of the nanoparticles. Isocyanates can react with any water present, releasing CO<sub>2</sub> and degrading into an amine, which can further react with other isocyanates, consuming the reactant before it is able to attach to a CNC surface. One approach to overcome this loss is using a significant excess of isocyanate to counter the water carried by CNCs.<sup>29</sup> An alternative approach that is commonly used in industry, particularly for waterborne polyurethanes, is the use of blocked isocyanates.<sup>30</sup> Such blocked isocyanates can dissociate at elevated temperatures to release the blocking group, regenerating the isocyanate to react with an appropriate hydroxyl or other nucleophilic moiety. For example, Chowdhury et al. utilized blocked isocyanate chemistry to incorporate CNCs into waterborne polyurethane coatings.<sup>31</sup> One class of blocked isocyanate is the hindered urea (HU), where the isocyanate is reacted with a bulky amine compound. Hindered urea moieties are dynamic bonds and have a range of dissociation temperatures depending on the bulkiness of the amine blocking group.<sup>32,33</sup>

In this work, a solvent-free “grafting-to” method is reported. By taking advantage of dynamic covalent HU chemistry, an isocyanate-terminated polymer is generated in-situ (Figure 1A), which can subsequently react with surface hydroxyl groups to form a urethane bond, thus functionalizing the CNCs (Figure 1B). The solvent-free nature of this reaction makes the technique more environmentally friendly and improves the scalability of the reaction since most industrial processes are conducted in the melt. This study first demonstrates the viability of the concept with model reactions, then translates the developed functionalization process toward the modification of CNCs with a range of polymers.

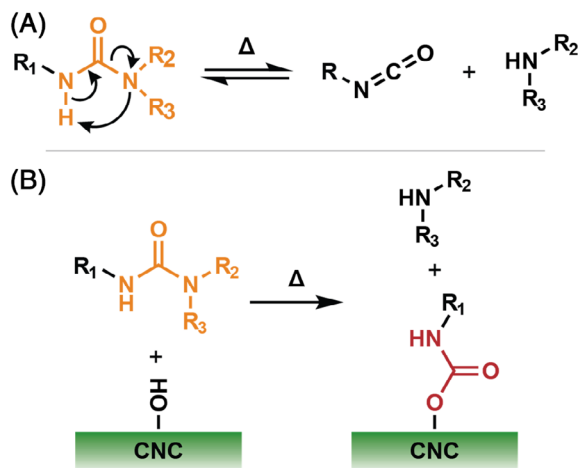


**FIGURE 1** (A) Schematic of a dynamic hindered urea motif and its dissociation into an isocyanate and secondary amine, and (B) a schematic of the reaction between a dynamic hindered urea and hydroxyl groups on the surface of cellulose nanocrystals, forming a urethane on the CNC surface and releasing the secondary amine.

## 2 | RESULTS AND DISCUSSION

When designing a hindered urea system for grafting onto CNCs, the dissociation temperature of the blocked isocyanate is a key consideration. Depending on surface functionality, CNCs can begin to degrade around 165 °C,<sup>34</sup> so the isocyanate must be regenerated below that limit. Depending on the amine group used to block the isocyanate, hindered urea groups can activate between 30 and 200 °C.<sup>33,35</sup> For this reason, *N-tert*-butylmethylamine was chosen as the blocking group because of its  $K_{eq}$  of roughly 90 M<sup>-1</sup> at 130 °C, which corresponds to about 8 mol.% hindered urea activation.<sup>35</sup> This activation temperature is above room temperature and the boiling point of water to limit premature reactions, but well below the CNC degradation threshold.

### 2.1 | Isolation and characterization of *c*-CNC-OSO<sub>3</sub> and *c*-CNC-COOH

Following a previously reported procedure,<sup>36</sup> cellulose nanocrystals were isolated from cotton-based cellulose filter paper using sulfuric acid (*c*-CNC-OSO<sub>3</sub>) and hydrochloric acid (*c*-CNC-OH) (see the supporting information (SI) for full experimental procedures). Following isolation, the *c*-CNC-OH nanoparticles were treated with (2,2,6,6-tetramethylpiperidin-1-yl)oxyl (TEMPO) to oxidize primary alcohol groups on the CNC surface into carboxylate groups, transforming *c*-CNC-OH into *c*-CNC-COOH. The resulting nanoparticles were freeze-dried for

easier handling before full characterization. In brief, atomic force microscopy (AFM) was used to measure the dimensions of the *c*-CNC-COOH to be 170 ± 80 nm in length, 23 ± 5 nm in width, and 10 ± 3 nm in height (Figures S1a and S1b). The dimensions of *c*-CNC-OSO<sub>3</sub> were 148 ± 93 nm, 60 ± 10 nm, and 8 ± 3 nm in length, width, and height, respectively (Figure S2a). Conductivity titration determined the surface carboxylate density to be 410 ± 60 mmol kg<sup>-1</sup> (Figure S1c) and surface sulfate density to be 285 ± 24 mmol kg<sup>-1</sup> (Figure S2b). Wide angle X-ray scattering (WAXS) measured the crystallinity index to be 0.67 (Figure S1d) for *c*-CNC-COOH and 0.85 for *c*-CNC-OSO<sub>3</sub> (Figure S2c). Finally, thermogravimetric analysis (TGA) showed a degradation onset ( $T_{d,95}$ ) of 226 °C for *c*-CNC-COOH (Figure S1e) and 175 °C for *c*-CNC-OSO<sub>3</sub> (Figure S2d).

### 2.2 | Reactions of alkyl hindered ureas with protected sugars and CNCs

To study the dissociation temperature of the selected hindered urea component, a series of model experiments were conducted with a hindered urea-terminated alkyl chain. Specifically, dodecyl isocyanate was reacted with *N-tert*-butylmethylamine in toluene to make dodecyl-HU. The dissociation of dodecyl-HU was monitored in the melt over a range of temperatures using in-situ Fourier Transform Infrared (FTIR) spectroscopy (Figure S3a). Dodecyl-HU was heated from 30 to 130 °C in increments of 10 °C, waiting 10 min between each increment. During this test, a characteristic isocyanate N=C=O stretching peak at 2270 cm<sup>-1</sup> began appearing around 100 °C, indicating the dissociation of hindered urea group and the evaporation of the *N-tert*-butylmethylamine (b.p. 69 °C) (Figure S3b). The intensity of the isocyanate band continued to increase with temperature up to 130 °C. Concomitantly, the hindered urea C=O stretching band at 1630 cm<sup>-1</sup> disappeared as a new band appeared at 1654 cm<sup>-1</sup>, corresponding to C=O stretching of the isocyanate (Figure S3b).

Prior to examining the ability of the dodecyl-HU to react with CNCs, a model experiment was carried out by reacting dodecyl-HU with 1,2:3,4-di-O-isopropylidene- $\alpha$ -D-galactopyranose (referred to as PG) (Figure 2A). PG is a protected galactose derivative with only the primary 5-hydroxyl group available for reaction, which allows for easier characterization of urethane bond formation.<sup>37</sup> Dodecyl-HU and PG were mixed in a 1:1 molar ratio using a minimal amount of acetone. The solvent was removed under high vacuum and the reaction proceeded in the melt at 120 °C for 5 h. The disappearance of the hindered urea and formation of the urethane compound

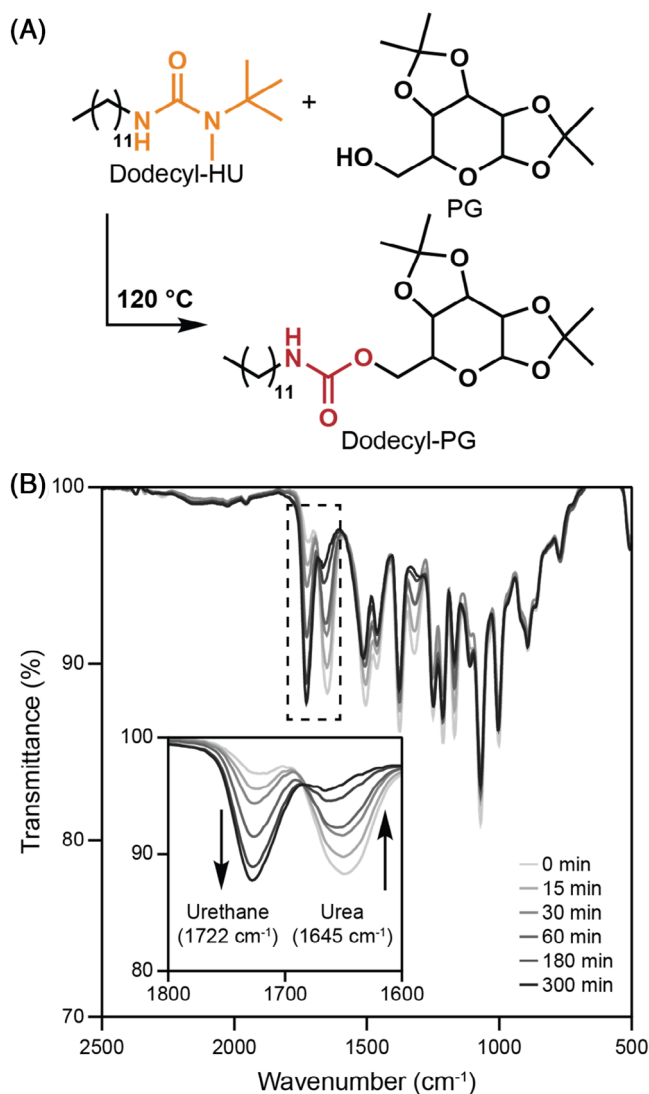


**FIGURE 2** (A) Schematic of the reaction between PG and dodecyl-HU to form a urethane bond and (B) the FTIR spectra of the reaction over time, showing the disappearance of the urea peak at  $1645\text{ cm}^{-1}$  and the appearance of the urethane peak at  $1722\text{ cm}^{-1}$ .

were monitored by in-situ FTIR (Figure 2B), highlighting the disappearance of the urea C=O stretching peak at  $1645\text{ cm}^{-1}$  and the concomitant appearance of the urethane C=O stretching peak at  $1722\text{ cm}^{-1}$ . It is worthwhile to note that no other significant peaks appear in the carbonyl region, suggesting that this reaction is relatively clean and avoids the formation of side products. Additionally, synthesis was confirmed with  $^1\text{H}$  NMR after purification (Figure S4).

The covalent attachment of dodecyl-HU to CNC was then explored by combining a 2:1 molar ratio of HU to surface alcohol groups on the *c*-CNC-OSO<sub>3</sub> (calculated based on prior literature<sup>15</sup>) in minimal acetone to blend the components (Figure 3A). In this initial test, sulfate-

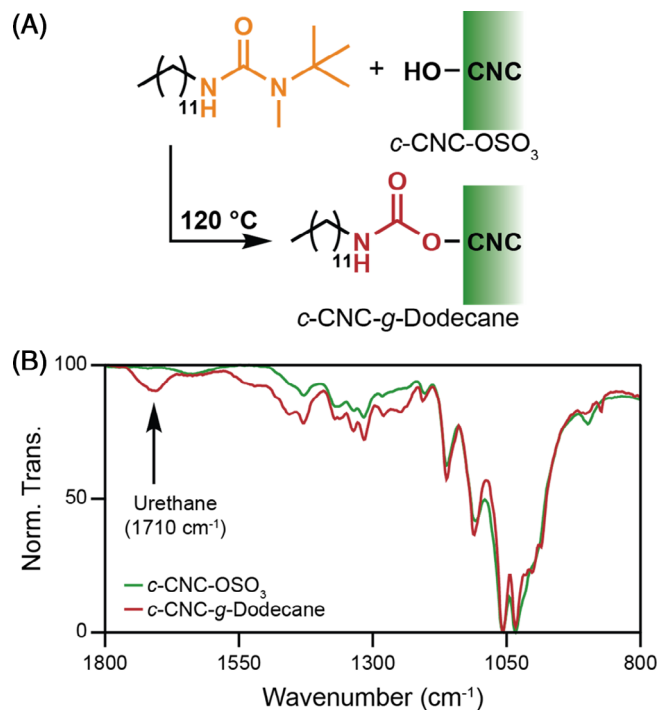


**FIGURE 3** (A) A schematic of the reaction between dodecyl-HU and surface alcohol groups on CNCs and (B) FTIR spectra of the resulting purified *c*-CNC-g-dodecane, highlighting the appearance of the urethane peak at  $1710\text{ cm}^{-1}$ .

functionalized CNCs were selected due to the presence of reactive primary hydroxyl groups as well as charged sulfate surface groups to promote dispersion and mixing.<sup>38</sup> After removing the acetone with vacuum, the bulk mixture was heated to 120 °C for 2 h to avoid CNC degradation at prolonged times. To characterize the grafting, it was necessary to remove the unreacted dodecyl-HU from the functionalized CNCs, which was achieved by washing the reaction mixture five times with acetone (see SI for full procedure). The resulting *c*-CNC-g-dodecane was characterized using FTIR, which showed the appearance of the urethane C=O peak at  $1710\text{ cm}^{-1}$  (Figure 3B). It is noteworthy that although the broadness of the urethane peak could indicate the formation of side products, such as allophanates,<sup>39</sup> the increased thermal stability of *c*-CNC-g-dodecane seen in the TGA curve still supports surface modification (Figure S5). While these measurements did not allow for quantification of the dodecyl group surface density, these results confirm a successful reaction between the CNCs and the small molecule hindered urea.

Having confirmed that it is possible to functionalize the CNC surface with a small molecule using dynamic hindered urea chemistry in the bulk, the next step was to explore the grafting of polymers onto CNC surfaces using this approach.

## 2.3 | Synthesis and characterization of hindered urea-terminated polymers

To demonstrate the versatility of this functionalization method, four polymers were chosen for functionalization onto CNC surfaces: poly(ethylene glycol) at 2000 and 10,000 g mol<sup>-1</sup> (PEG<sub>2k</sub> and PEG<sub>10k</sub>) as well as polycaprolactone (PCL<sub>10k</sub>) and poly(butyl acrylate) (PBA<sub>10k</sub>), both at 10,000 g mol<sup>-1</sup>. PEG was chosen to allow comparison with previously reported solution-based “grafting-to” chemistries that have been used to synthesize PEG-grafted CNCs,<sup>15</sup> bio-based PCL was chosen to highlight the ability to make fully sustainable nanoparticles, and PBA was chosen to highlight the ability to functionalize and graft polymers synthesized via controlled, living polymerization techniques.

### 2.3.1 | Synthesis and characterization of PEG-HU and PCL-HU

After purchasing and synthesizing<sup>40</sup> PEG-OH and PCL-OH respectively (see SI for synthetic details), the next step was to create hindered urea-terminated polymers. For simplicity, discussion about synthesis and characterization will focus on PEG<sub>2k</sub>, but reaction conditions and observations were similar between all PEG and PCL materials. Isocyanate-terminated PEG<sub>2k</sub> (PEG<sub>2k</sub>-NCO) was synthesized at 40 °C in dry toluene using an excess of hexamethylene diisocyanate and dibutyltin dilaurate (DBTDL) as catalyst (Figure 4A). During the work-up of this intermediate, it was vital to maintain an inert atmosphere and keep the material as cold as possible. Even brief exposure to atmospheric conditions resulted in impurities in the final product. Once the PEG<sub>2k</sub>-NCO had been reacted with *N-tert*-butylmethylamine (Figure 4A), the resulting hindered urea-terminated PEG<sub>2k</sub> (PEG<sub>2k</sub>-HU) was much more stable and could be stored at ambient conditions for an extended period. The same phenomena were also observed when synthesizing PEG<sub>10k</sub>-NCO and PEG<sub>10k</sub>-HU as well as PCL<sub>10k</sub>-NCO and PCL<sub>10k</sub>-HU.

PEG<sub>2k</sub>-NCO was characterized with FTIR (Figure 4B), size exclusion chromatography (SEC) (Figure S6a), and <sup>1</sup>H NMR (Figure S6b) to verify its structure prior to protecting the isocyanate with the secondary amine. Once protected with *N-tert*-butylmethylamine, <sup>1</sup>H NMR was repeated to confirm the appearance of peaks at 2.81 and 1.39 ppm, corresponding to the methyl and *tert*-butyl groups of the HU, respectively (Figure S6b). Additionally, the appearance of the urea peak at 1631 cm<sup>-1</sup> in FTIR confirmed successful synthesis (Figure 4B). Shoulders around the urethane peak imply that isocyanate side reactions could be occurring, such as the formation of allophanates and

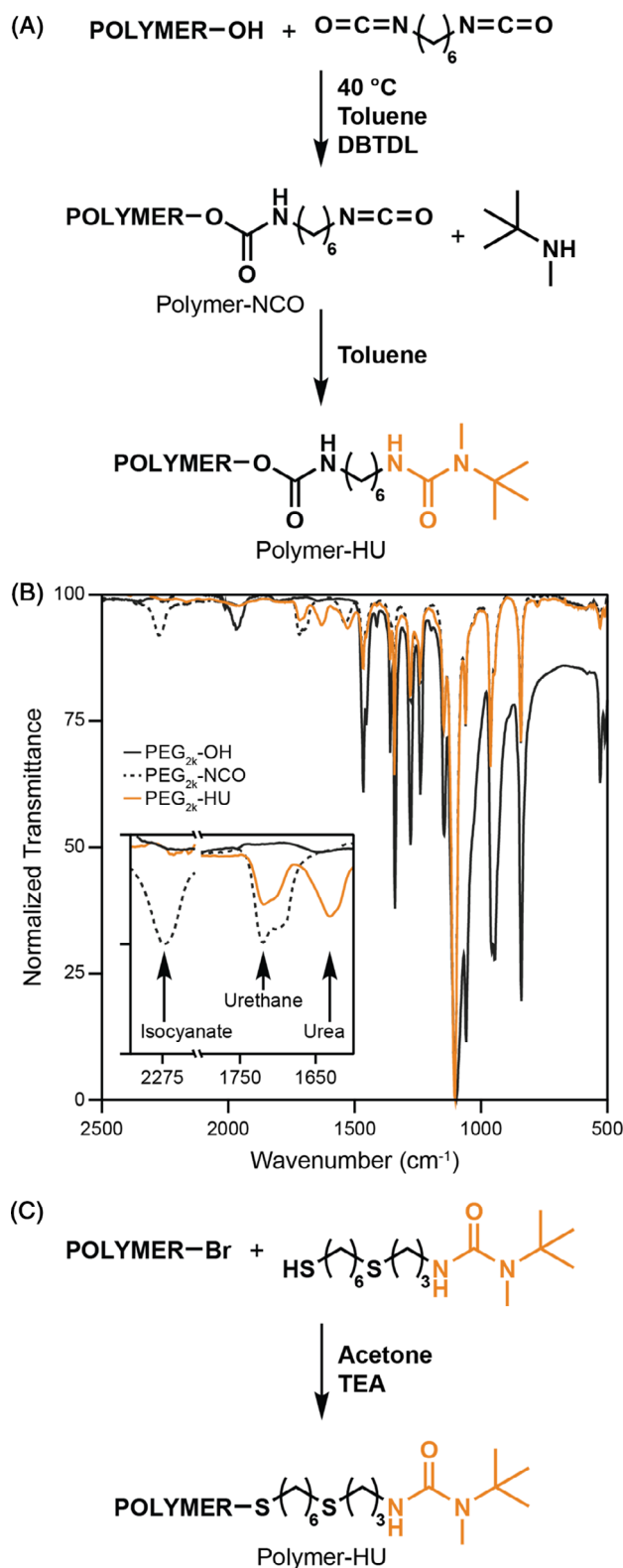


**FIGURE 4** (A) Schematic for the conversion of polymers with alcohol end groups into hindered urea-terminated polymers, (B) FTIR spectra of PEG<sub>2k</sub>-OH, PEG<sub>2k</sub>-NCO, and PEG<sub>2k</sub>-HU showing the appearance of the isocyanate peak at 2272 cm<sup>-1</sup> in PEG<sub>2k</sub>-NCO and the urea peak at 1631 cm<sup>-1</sup> in PEG<sub>2k</sub>-HU, and (C) a schematic for the conversion of polymers with bromine end groups into hindered urea-terminated polymers.

biurets. This is further suggested by the presence of a small peak in the SEC that is roughly double the initial polymer mass (Figure S6a). While the presence of these components would impact the stoichiometry of grafting reactions, their relatively small mass fraction (15 wt.% based on the PEG<sub>2k</sub>-HU SEC peak) means that these are minor side reactions. Similar characterization was conducted on PEG<sub>10k</sub>-NCO and -HU as well as PCL<sub>10k</sub>-NCO and -HU (Figures S7 and S8).

### 2.3.2 | Synthesis and characterization of PBA-HU

Synthesis of bromine-terminated PBA-Br was achieved using Cu(0)-mediated living radical polymerization with ethyl  $\alpha$ -bromoisobutyrate as the initiator (Figure S9) (see SI for full experimental procedures).<sup>41</sup> To substitute a hindered urea group onto the bromine chain end, a thiol-functionalized hindered urea was synthesized by blocking allyl isocyanate with *N*-tert-butylmethylamine (Figure S10). Then, thiol-ene click chemistry was used with an excess of 1,6-hexanedithiol to generate the desired thio-HU small molecule (Figure S11). Finally, nucleophilic substitution was conducted between the thio-HU and bromine end group to connect the hindered urea to the polymer chain (Figure 4C). After purification of PBA-HU, SEC showed a small shift to shorter retention times, consistent with the substitution of the bromine by the thio-HU moiety (Figure S9a). Additionally, <sup>1</sup>H NMR showed the appearance of the methyl and tert-butyl group peaks at 2.81 and 1.39 ppm respectively (Figure S9b).

## 2.4 | Preparation, characterization, and optimization of PEG<sub>2k</sub>-grafted *c*-CNCs

In prior work, it has been shown that it is possible to quantify the amount of PEG grafted to CNC-COOH using dynamic thermogravimetric analysis.<sup>15</sup> During initial HU-terminated polymer grafting tests using sulfate-functionalized *c*-CNC-OSO<sub>3</sub>, it was found that the broader degradation range of the *c*-CNC-OSO<sub>3</sub> (Figure S2d) made quantification of the polymer content on the grafted nanoparticles difficult via TGA. For this reason, grafting to *c*-CNC-COOH with a narrower degradation window (Figure S1e) was adopted, resulting in better separation of cellulose and PEG degradation via thermogravimetry. The key difference between these types of CNC is the presence of the more reactive primary hydroxyl groups on the *c*-CNC-OSO<sub>3</sub>, whereas most of the primary alcohols have been converted to carboxylate groups on the *c*-CNC-COOH.

However, isocyanates can also react with the secondary alcohols on a sugar unit, albeit at a lower rate.<sup>42</sup>

To prepare for grafting, freeze-dried *c*-CNC-COOH were dispersed in water at a concentration of 5 mg mL<sup>-1</sup> and solvent exchanged into acetone. Using PEG<sub>2k</sub> as a preliminary sample, 400 mg (approx. 2.7 mol eq. relative to surface -OH groups) of PEG<sub>2k</sub>-HU were dissolved in the CNC dispersion per 100 mg of *c*-CNC-COOH. The acetone was then removed under high vacuum at ambient temperature. The resulting powder was melted at 120 °C and stirred for 2 h under vacuum (120 mbar) to remove the volatile amine and yield *c*-CNC-g-PEG<sub>2k</sub> (Figure 5A).

To explore the effects of the amine blocking group on CNC grafting, grafting was also conducted with PEG<sub>2k</sub>-NCO (Figure 5B). Experimentally, the procedure was identical to PEG<sub>2k</sub>-HU grafting, but was done immediately after PEG<sub>2k</sub>-NCO preparation to avoid any loss of the isocyanate that could occur from hydrolysis or other side reactions during storage. Grafting was conducted under vacuum on an FTIR thermal stage so that spectra could be gathered in-situ. The resulting spectra for PEG<sub>2k</sub>-NCO (Figure 5C) highlights the proclivity of the isocyanate to undergo side reactions with large shoulders appearing around 1765 and 1700 cm<sup>-1</sup> in the grafted sample (Figure 5C inset). These peaks likely correspond to uretdione<sup>43</sup> and allophanate<sup>39</sup> production, respectively. The PEG<sub>2k</sub>-HU-grafted sample shows notably smaller shoulders (Figure 5D). To quantify these differences, the decrease of the isocyanate (2275 cm<sup>-1</sup>) and urea (1655 cm<sup>-1</sup>) reactant peaks is plotted against time along with the increase of the product urethane peak (1722 cm<sup>-1</sup>). In an ideal system, the consumption of reactants should translate directly into product growth, indicating inhibition of any side reactions taking place. For grafting with PEG-NCO (Figure 5E), these two curves diverge within the first 30 min of the reaction, which suggests that the isocyanate moiety is undergoing side reactions. In contrast, the PEG-HU grafting curves (Figure 5F) show a slower, steadier consumption of the hindered urea peak and a corresponding increase in the urethane peak throughout the reaction. This data is consistent with slower, more controlled grafting with the hindered urea relative to the unblocked isocyanate.

To confirm that the polymer chains were indeed grafted to the CNCs, it is important to remove any unreacted polymer and carry out detailed characterization of the degree of functionalization on the polymer-grafted CNCs. To ensure thorough removal of excess unreacted polymer after surface functionalization, a diagnostic test was done by adding dye-tagged PEG to the reaction after completion and tracking the amount of dye remaining in the product after each wash (Figure S12). It was found that the most effective washing method for PEG removal was a 1:1 mixture of acetone: water. After 12 centrifugation and resuspension cycles, no residual

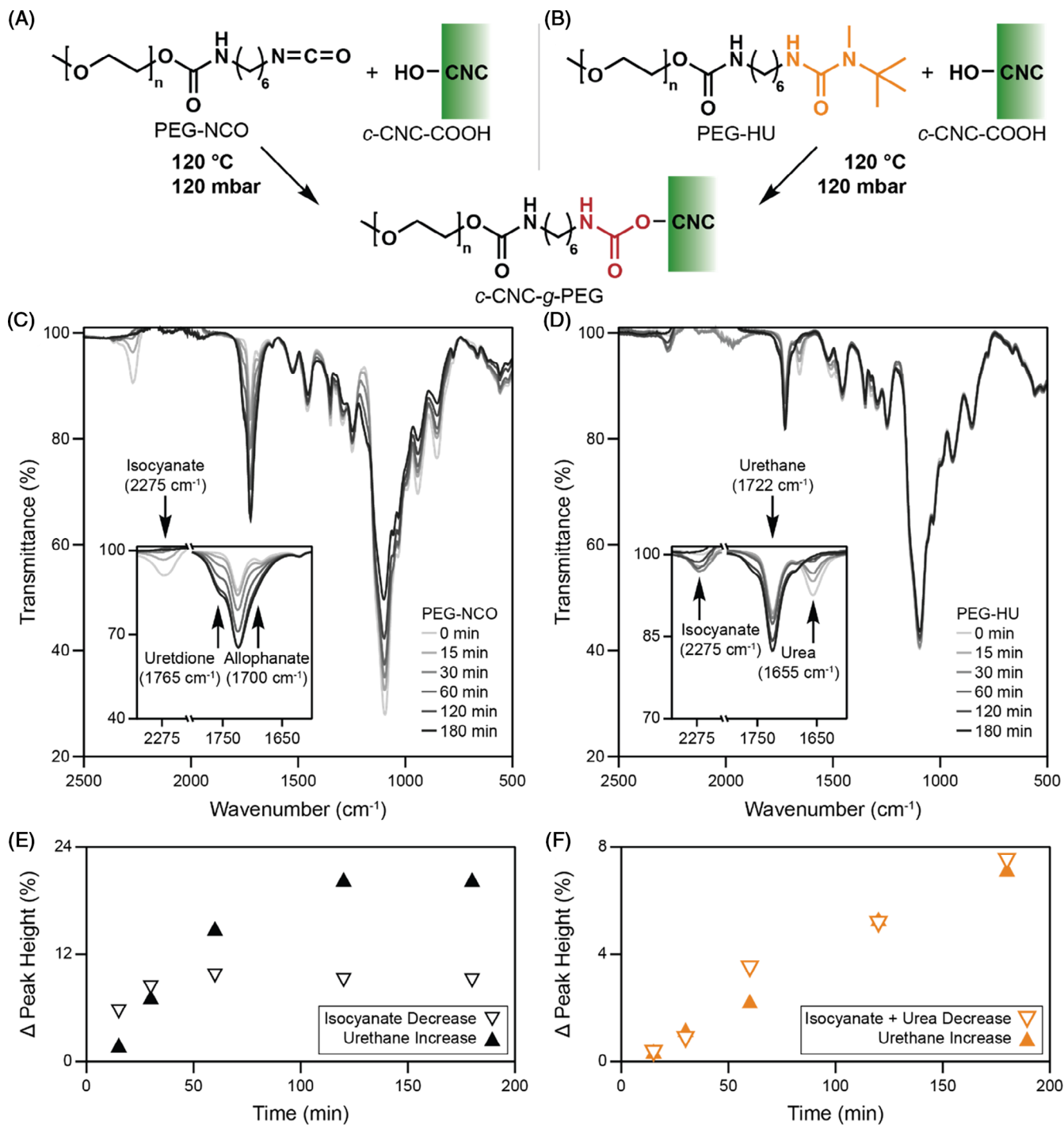


**FIGURE 5** (A) Schematic of grafting PEG-NCO onto the hydroxyl groups of CNCs, (B) schematic of grafting PEG-HU onto the hydroxyl groups of CNCs, (C) time-resolved FTIR of PEG<sub>2k</sub>-NCO grafting to *c*-CNC-COOH highlighting the shoulders appearing around the urethane peak, (D) time-resolved FTIR of PEG<sub>2k</sub>-HU grafting to *c*-CNC-COOH with no such shoulders, (E) change in reactant (isocyanate) and product (urethane) peak heights plotted against time for PEG<sub>2k</sub>-NCO grafting, and (F) change in reactant (isocyanate + urea) and product (urethane) peak heights plotted against time for PEG<sub>2k</sub>-HU grafting.

dye could be detected in the supernatant, implying that most, if not all, of the non-attached polymer chains had been removed. This strategy was then employed for the removal of untagged free polymer chains in all other samples.

After thorough cleaning, the amount of grafted polymer was measured using high resolution, dynamic TGA. Dynamic TGA is a procedure that slows the heating rate of the experiment whenever a mass loss event is detected, which helps to isolate individual degradation events. This

method allowed for enhanced separation of CNC and polymer degradation, allowing for more accurate quantification of polymer content via thermogravimetry (Figure 6A).<sup>44</sup> By

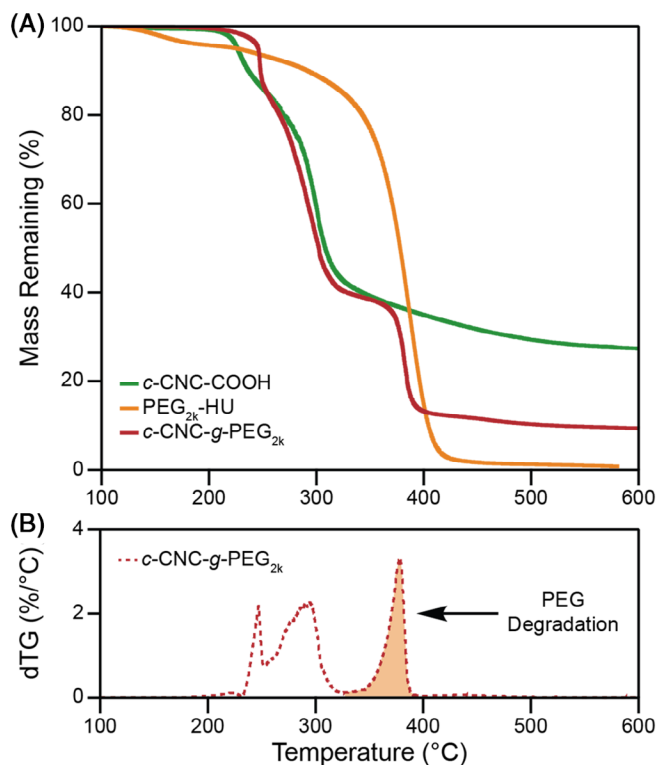


**FIGURE 6** (A) TGA degradation curves of *c*-CNC-COOH, PEG<sub>2k</sub>-HU, and a characteristic sample of *c*-CNC-g-PEG<sub>2k</sub> and (B) the derivative of the *c*-CNC-g-PEG<sub>2k</sub> degradation curve, highlighting the separation of CNC degradation and PEG degradation (shaded).

taking the derivative of the mass loss and interpolating a line between the points at 330 and 400 °C to account for baseline CNC degradation, the PEG mass fraction could be determined via integration of the degradation peak (Figures 6B and S13) and used to calculate the surface grafting density based on the crystal structure of cellulose and the CNC dimensions measured via AFM.<sup>15,45</sup>

With characterization established, a series of experiments were done to optimize the reaction conditions for grafting PEG<sub>2k</sub>-HU to *c*-CNC-COOH by varying the reaction time, reaction temperature, and ratio of polymer to surface hydroxyl groups (Table 1). The model reactions discussed earlier helped to define upper and lower limits for these tests, with 2 h, 120 °C, and 400 mg PEG for every 100 mg *c*-CNC-COOH being considered the baseline conditions. From these studies, 2 h was found to be the optimal reaction time, with shorter reactions not allowing for full HU conversion and longer reactions allowing more time for side reactions to reduce grafting density. The optimal reaction temperature was found to be 130 °C, with lower temperatures not activating the hindered urea groups efficiently enough and higher temperatures promoting side reactions.

While it was expected that grafting efficiency would decrease as the ratio of polymer to *c*-CNC-COOH mass increased, it was found that the grafting density plateaued above 200 mg of PEG<sub>2k</sub>-HU. It is possible that the higher ratio of polymer chains results in an increased concentration of isocyanate groups that can react with each other rather than the CNC surface. Additionally, steric bulk at the CNC surface may provide a physical limit as more polymer chains attach to the nanoparticles.

**TABLE 1** An array of *c*-CNC-g-PEG<sub>2k</sub> grafting reaction conditions and the resulting reaction efficiencies and grafting densities.

<i>c</i> -CNC-COOH [mg]	PEG <sub>2k</sub> -HU [mg (mol eq.) <sup>a</sup> ]	Time [h]	Temperature [°C]	Reaction efficiency [% of chains grafted]	Grafting density [chains nm <sup>-2</sup> ]
100	400 (2.7)	1.5	120	4.6	0.30
100 <sup>b</sup>	400 (2.7)	2	120	6.6	0.42
100	400 (2.7)	3	120	4.9	0.32
100	400 (2.7)	4	120	2.3	0.14
100	400 (2.7)	2	110	4.7	0.30
100 <sup>b</sup>	400 (2.7)	2	120	6.6	0.42
100	400 (2.7)	2	130	7.4	0.47
100	400 (2.7)	2	140	4.6	0.30
100	100 (0.7)	2	120	15.4	0.25
100	200 (1.4)	2	120	13.8	0.44
100 <sup>b</sup>	400 (2.7)	2	120	6.6	0.42
100	800 (5.4)	2	120	2.8	0.36
100	1600 (10.9)	2	120	1.2	0.30

<sup>a</sup>Molar equivalent relative to surface alcohol groups on the *c*-CNC-COOH.

<sup>b</sup>Denotes the same baseline data, repeated for clarity.



By reducing the polymer: CNC ratio further to 1:1 by mass, too few polymer chains are present in the system, causing grafting density to be reduced from 0.44 to 0.25 chains  $\text{nm}^{-2}$ . In fact, varying the polymer: CNC mass ratio allows access to *c*-CNC-*g*-PEG<sub>2k</sub> with grafting densities that range from 0.25 to 0.44 chains  $\text{nm}^{-2}$ . It is worth noting that the reaction efficiency (polymer grafted vs. polymer added to the reaction) is better at lower polymer: CNC mass ratios. The optimized reaction conditions for PEG<sub>2k</sub> grafting (1.4 eq. of polymer relative to surface hydroxyl groups, 2 h reaction time, and 130 °C) were used to graft all other polymers to the CNC surface to allow for comparison.

## 2.5 | Results and analysis of grafting with a variety of polymers

To explore the versatility of this technique, grafting was also carried out with HU-terminated PEG<sub>10k</sub>, PCL<sub>10k</sub>, and PBA<sub>10k</sub> in addition to PEG<sub>2k</sub> with the established optimized conditions. For PCL and PBA-grafted CNCs, the cleaning washes were done with THF, which is a good solvent for both polymers.

It was not possible to determine the amount of PCL in the *c*-CNC-*g*-PCL<sub>10k</sub> samples using dynamic TGA as PCL degradation could not be deconvoluted from CNC degradation. Thus, an FTIR calibration curve was created by mixing varying ratios of PCL and CNCs and measuring the relative intensity of the 1724  $\text{cm}^{-1}$  peak in the normalized spectra, corresponding to the carbonyl group in the PCL repeat unit (Figure 7). When plotted against PCL content, the peak heights generated a linear relation that could be used to estimate grafted PCL content (Figure 7 inset). For PBA, both dynamic TGA and FTIR calibration curves were used to quantify the grafted polymer content, and both methods corroborated each other (Figures S14 and S15).

The results for grafting all polymers with the optimized conditions can be seen in Table 2. Putting these results in the context of other grafting methods, prior work from Rowan and coworkers used peptide coupling in DMF to access PEG-grafted CNCs.<sup>15</sup> With PEG<sub>2k</sub>, the best reaction conditions resulted in a grafting density of 0.33 chains  $\text{nm}^{-2}$ . This work observed a grafting density of 0.46 chains  $\text{nm}^{-2}$  using the optimized conditions, which is notably higher than the grafting density achieved in solution. It is, of course, important to note that the isocyanates can react with the 2- and 3-hydroxyl groups on the cellulose unit, whereas only the primary 6-hydroxyl can react with the amine during peptide coupling. It is possible to use the hindered urea grafting approach to replicate the solution grafting density

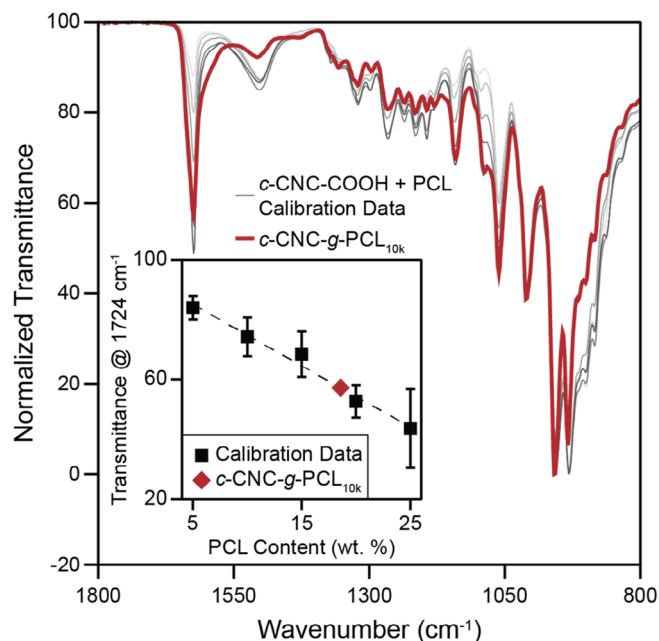


**FIGURE 7** FTIR data for *c*-CNC-COOH mixed with PCL<sub>10k</sub>-OH at various ratios along with the resulting calibration curve (inset) with the polymer-grafted *c*-CNC-*g*-PCL<sub>10k</sub> overlaid on both.

**TABLE 2** Grafting results for a variety of polymers onto *c*-CNC-COOH using optimized grafting conditions.

Sample	Polymer mass fraction [wt. %]	Grafting density [chains/ $\text{nm}^2$ ]
<i>c</i> -CNC- <i>g</i> -PEG <sub>2k</sub>	22.4 <sup>a</sup>	0.46
<i>c</i> -CNC- <i>g</i> -PEG <sub>10k</sub>	24.5 <sup>a</sup>	0.10
<i>c</i> -CNC- <i>g</i> -PCL <sub>10k</sub>	18.6 <sup>b</sup>	0.07
<i>c</i> -CNC- <i>g</i> -PBA <sub>10k</sub>	8.7 <sup>b</sup>	0.03

<sup>a</sup>Measured via dynamic TGA.

<sup>b</sup>Measured via FTIR calibration curve.

reported in this prior literature using half as much polymer reactant by mass.

For PEG<sub>10k</sub> grafting, the resulting grafting density was 0.10 chains  $\text{nm}^{-2}$ , which is lower than the PEG<sub>2k</sub>-grafted sample presumably on account of the steric bulk of the larger polymer chains, as seen in prior work.<sup>15</sup> Compared to the highest solution grafting density results of 0.07 chains  $\text{nm}^{-2}$  for PEG<sub>10k</sub>, the hindered urea grafting method developed herein is able to achieve greater grafting densities than solution-based grafting methods.<sup>15</sup> Composites with PLA were prepared for the PEG<sub>2k</sub> and PEG<sub>10k</sub>-grafted CNCs and were shown to exhibit properties similar to those seen in prior solution-grafted CNC composites (Figure S16).<sup>15</sup>

Based on the FTIR calibration curve for *c*-CNC-*g*-PCL<sub>10k</sub>, the calculated grafting density of 0.07 chains

$\text{nm}^{-2}$  is slightly lower than the  $\text{PEG}_{10\text{k}}$  grafting density. While the different polymer structures make these results difficult to compare, it is hypothesized that the reduced flexibility of the polycaprolactone chain (Kuhn length  $b = 10.0 \text{ \AA}$  for PCL<sup>46</sup> vs.  $b = 7.6 \text{ \AA}$  for PEG<sup>47</sup>) likely increases the steric hinderance at the nanoparticle surface, resulting in fewer polymer chains finding a reactive site on the CNC. Nearly all PCL-grafted CNCs in literature are synthesized via ring opening polymerization from the CNC surface, which is a technique that makes it difficult to characterize the grafted chain length or density. As an elementary comparison, a few reports have used FTIR to characterize their PCL-grafted CNCs and the relative intensity of the  $1724 \text{ cm}^{-1}$  peak corresponding to the carbonyl in the PCL backbone is roughly similar to the relative intensity observed here (Figure 7), suggesting that the PCL content of the resulting nanoparticles is competitive with grafting-from techniques.<sup>11,48,49</sup>

Finally,  $\text{PBA}_{10\text{k}}$  grafting resulted in  $0.03 \text{ chains nm}^{-2}$ , which is notably lower than the  $\text{PEG}_{10\text{k}}$  and  $\text{PCL}_{10\text{k}}$  counterparts. This reduction in grafting density has been attributed to a further increase in the steric bulk from the butyl pendant group, as highlighted by a further increase in the Kuhn length to  $b = 17.1 \text{ \AA}$  for PBA.<sup>40</sup> Additionally, the more hydrophobic nature of this polymer may hinder mixing during the melt grafting process, further limiting surface functionalization. Regardless, the FTIR and TGA traces (Figures S14 and S15) show clear evidence of grafting, and the synthesis method is potentially applicable to a wide range of bromine-terminated polymers.

### 3 | CONCLUSIONS









Taking inspiration from the polyurethane industry, a method has been developed for the melt-functionalization of cellulose nanocrystals. By installing dynamic hindered urea moieties on the end of polymer chains, isocyanate groups were formed in-situ in the bulk. The isocyanate groups generated were able to react with surface hydroxyl groups on the CNCs, linking the polymer to the nanoparticle via a urethane linkage. The efficacy of the reaction was verified with a model small molecule system before being optimized with hindered urea-terminated  $\text{PEG}_{2\text{k}}$  chains on cotton-based, TEMPO-oxidized CNCs. Compared to the unblocked isocyanate, the hindered urea-functionalized polymer chains showed fewer side reactions, emphasizing the increased synthetic control afforded by the blocked system. The resulting polymer-grafted nanoparticles exhibited grafting densities that were superior to solution-based functionalization methods without the need for harmful solvents during the grafting reaction. Finally, the versatility of this method was highlighted by grafting CNC surfaces

with hindered urea-terminated dodecane,  $\text{PEG}_{10\text{k}}$ ,  $\text{PCL}_{10\text{k}}$ , and  $\text{PBA}_{10\text{k}}$ . Each of the resulting polymer-grafted nanoparticles showed polymer contents that were competitive with literature. Sustainable and efficient processing are crucial characteristics for polymer-grafted CNC to achieve commercial success going forward, and this method advances both of those metrics while achieving strong grafting densities with a range of polymers.

### ACKNOWLEDGMENTS

Z. Oluz and N. Macke contributed equally to this work. Materials, Methods, and Instrumentation details can be found in the supporting information. The authors gratefully acknowledge financial support through the National Science Foundation (NSF) Center for Sustainable Polymers (CSP) (CHE-1901635) and the Swiss National Science Foundation (SNSF) (P2FRP2\_181437). Parts of this work utilized the University of Chicago Materials Research Science and Engineering Center (NSF DMR-2011854), the University of Chicago NMR Facility, the University of Chicago Soft Matter Characterization Facility, and the University of Chicago X-ray facilities.

### ORCID

Zehra Oluz  <https://orcid.org/0000-0003-1287-383X>  
Nicholas Macke  <https://orcid.org/0000-0001-5072-7441>  
Sarah Candelaria  <https://orcid.org/0000-0001-5318-4649>  
Abrianna Ambus  <https://orcid.org/0009-0007-2415-0862>  
Aurora Zemborain  <https://orcid.org/0000-0002-0505-9891>  
Adam M. Weiss  <https://orcid.org/0000-0002-4972-1402>  
Céline Calvino  <https://orcid.org/0000-0001-8582-6108>  
Stuart J. Rowan  <https://orcid.org/0000-0001-8176-0594>

### REFERENCES

- [1] C. Calvino, N. Macke, R. Kato, S. J. Rowan, *Prog. Polym. Sci.* **2020**, *103*, 101221.
- [2] A. Dufresne, *Int. Polym. Process.* **2012**, *27*, 557.
- [3] R. J. Moon, A. Martini, J. Nairn, J. Simonsen, J. P. Youngblood, *Chem. Soc. Rev.* **2011**, *40*, 3941.
- [4] S. Chanda, D. S. Bajwa, *Rev. Adv. Mater. Sci.* **2021**, *60*, 325.
- [5] Y. Habibi, L. A. Lucia, O. J. Rojas, *Chem. Rev.* **2010**, *110*, 3479.
- [6] N. Dhar, D. Au, R. C. Berry, K. C. Tam, *Colloids Surf. A Physicochem. Eng. Asp.* **2012**, *415*, 310.
- [7] H. R. Paul, M. K. Bera, N. Macke, S. J. Rowan, M. V. Tirrell, *ACS Nano* **2024**, *18*, 1921.
- [8] S. Eyley, W. Thielemans, *Nanoscale* **2014**, *6*, 7764.
- [9] J. C. Natterodt, A. Petri-fink, C. Weder, J. O. Zoppe, *Chimia* **2017**, *71*, 376.
- [10] Y. Habibi, *Chem. Soc. Rev.* **2014**, *43*, 1519.
- [11] S. Wohlhauser, G. Delepierre, M. Labet, G. Morandi, W. Thielemans, C. Weder, J. O. Zoppe, *Macromolecules* **2018**, *51*, 6157.

- [12] S. A. Kedzior, J. O. Zoppe, R. M. Berry, E. D. Cranston, *Curr. Opin. Solid State Mater. Sci.* **2019**, *23*, 23.
- [13] E. Lizundia, E. Meaurio, J. L. Vilas, *Multifunctional Polymeric Nanocomposites Based on Cellulosic Reinforcements*, Elsevier, Norwich, **2016**, p. 61.
- [14] N. Macke, C. M. Hemmingsen, S. J. Rowan, *J. Polym. Sci.* **2022**, *60*, 3318.
- [15] L. Geurds, J. Lauko, A. E. Rowan, N. Amiralian, *J. Mater. Chem. A* **2021**, *9*, 17173.
- [16] S. Minko, *Polymer Surfaces Interfaces*, Springer, Berlin, **2008**, p. 215.
- [17] P. V. Kelly, S. Shams Es-haghi, M. E. Lamm, K. Copenhaver, S. Ozcan, D. J. Gardner, W. M. Gramlich, *ACS Appl. Polym. Mater.* **2023**, *5*, 3661.
- [18] S. Wohlhauser, C. Rader, C. Weder, *Biomacromolecules* **2022**, *23*, 699.
- [19] B. Zdyrko, I. Luzinov, *Macromol. Rapid Commun.* **2011**, *32*, 859.
- [20] R. Kato, J. H. Lettow, S. N. Patel, S. J. Rowan, *ACS Appl. Mater. Interfaces* **2020**, *12*, 54083.
- [21] H. R. Paul, M. V. Tirrell, S. J. Rowan, *ACS Appl. Nano Mater.* **2024**, *7*, 4210.
- [22] J. H. Lettow, H. Yang, P. F. Nealey, S. J. Rowan, *Macromolecules* **2021**, *54*, 10594.
- [23] F. Azzam, L. Heux, J.-L. Putaux, B. Jean, *Biomacromolecules* **2010**, *11*, 3652.
- [24] E. Kloser, D. G. Gray, *Langmuir* **2010**, *26*, 13450.
- [25] A. Pei, J.-M. Malho, J. Ruokolainen, Q. Zhou, L. A. Berglund, *Macromolecules* **2011**, *44*, 4422.
- [26] D. Viet, S. Beck-Candanedo, D. G. Gray, *Cellulose* **2007**, *14*, 109.
- [27] J. O. Akindoyo, M. D. H. Beg, S. Ghazali, M. R. Islam, N. Jeyaratnam, A. R. Yuvaraj, *RSC Adv.* **2016**, *6*, 114453.
- [28] H. Abushammala, *Polymers* **2019**, *11*, 1.
- [29] Z. W. Wicks, *Prog. Org. Coatings* **1975**, *3*, 73.
- [30] R. A. Chowdhury, C. M. Clarkson, S. Shrestha, S. M. El Awad Azrak, M. Mavlan, J. P. Youngblood, *ACS Appl. Polym. Mater.* **2020**, *2*, 385.
- [31] Q. Zhang, S. Wang, B. Rao, X. Chen, L. Ma, C. Cui, Q. Zhong, Z. Li, Y. Cheng, Y. Zhang, *React. Funct. Polym.* **2021**, *159*, 104807.
- [32] H. Ying, Y. Zhang, J. Cheng, *Nat. Commun.* **2014**, *5*, 3218.
- [33] O. M. Vanderfleet, M. S. Reid, J. Bras, L. Heux, J. Godoy-Vargas, M. K. R. Panga, E. D. Cranston, *Cellulose* **2019**, *26*, 507.
- [34] L. Zhang, S. J. Rowan, *Macromolecules* **2017**, *50*, 5051.
- [35] A. M. Weiss, N. Macke, Y. Zhang, C. Calvino, A. P. Esser-Kahn, S. J. Rowan, *ACS Biomater. Sci. Eng.* **2021**, *7*, 1450.
- [36] A. Gille, M. Hiersemann, *Org. Lett.* **2010**, *12*, 5258.
- [37] K. Oksman, Y. Aitomäki, A. P. Mathew, G. Siqueira, Q. Zhou, S. Butylina, S. Tanpichai, X. Zhou, S. Hooshmand, *Compos. Part A Appl. Sci. Manuf.* **2016**, *83*, 2.
- [38] E. Delebecq, J. Pascault, B. Boutevin, F. Ganachaud, *Chem. Rev.* **2013**, *113*, 80.
- [39] B. G. G. Lohmeijer, R. C. Pratt, F. Leibfarth, J. W. Logan, D. A. Long, A. P. Dove, F. Nederberg, J. Choi, C. Wade, R. M. Waymouth, J. L. Hedrick, *Macromolecules* **2006**, *39*, 8574.
- [40] A. Anastasaki, V. Nikolaou, G. Nurumbetov, P. Wilson, K. Kempe, J. F. Quinn, T. P. Davis, M. R. Whittaker, D. M. Haddleton, *Chem. Rev.* **2016**, *116*, 835.
- [41] L. Nagy, B. Vadkerti, G. Batta, P. P. Fehér, M. Zsuga, S. Kéki, *New J. Chem.* **2019**, *43*, 15316.
- [42] J. Hu, Z. Chen, Y. He, H. Huang, X. Zhang, *Res. Chem. Intermed.* **2017**, *43*, 2799.
- [43] K. Mohamed, *TA Instruments* **2016**, 122.
- [44] S. Elazouzi-Hafraoui, Y. Nishiyama, J.-L. Putaux, L. Heux, F. Dubreuil, C. Rochas, *Biomacromolecules* **2008**, *9*, 57.
- [45] D. Herrera, J.-C. Zamora, A. Bello, M. Grimau, E. Laredo, A. J. Müller, T. P. Lodge, *Macromolecules* **2005**, *38*, 5109.
- [46] L. J. Fetters, D. J. Lohse, D. Richter, T. A. Witten, A. Zirkel, *Macromolecules* **1994**, *27*, 4639.
- [47] C. Tian, S. Y. Fu, Q. J. Meng, L. A. Lucia, *Cellulose* **2016**, *23*, 2457.
- [48] Q. Huang, J. Huang, P. R. Chang, *Wuhan Univ. J. Nat. Sci.* **2014**, *19*, 117.
- [49] C. Frascini, G. Chauve, J. Bouchard, *Cellulose* **2017**, *24*, 2775.

## SUPPORTING INFORMATION

Additional supporting information can be found online in the Supporting Information section at the end of this article.

**How to cite this article:** Z. Oluz, N. Macke, S. Candelaria, A. Ambus, A. Zemborain, C. S. Udemgba, A. M. Weiss, C. Calvino, S. J. Rowan, *J. Polym. Sci.* **2024**, *1*. <https://doi.org/10.1002/pol.20240452>